

RESEARCH ARTICLE

Repurposing the *Streptococcus mutans* CRISPR-Cas9 System to Understand Essential Gene Function

Robert C. Shields^{1*}, Alejandro R. Walker¹, Natalie Maricic¹, Brinta Chakraborty¹, Simon A. M. Underhill², Robert A. Burne¹

1 Department of Oral Biology, College of Dentistry, University of Florida, Gainesville, Florida, United States of America, **2** Department of Physics, University of Florida, Gainesville, Florida, United States of America

* rshields@dental.ufl.edu



OPEN ACCESS

Citation: Shields RC, Walker AR, Maricic N, Chakraborty B, Underhill SAM, Burne RA (2020) Repurposing the *Streptococcus mutans* CRISPR-Cas9 System to Understand Essential Gene Function. PLoS Pathog 16(3): e1008344. <https://doi.org/10.1371/journal.ppat.1008344>

Editor: Paul M. Sullam, University of California, San Francisco, UNITED STATES

Received: October 3, 2019

Accepted: January 22, 2020

Published: March 9, 2020

Copyright: © 2020 Shields et al. This is an open access article distributed under the terms of the [Creative Commons Attribution License](https://creativecommons.org/licenses/by/4.0/), which permits unrestricted use, distribution, and reproduction in any medium, provided the original author and source are credited.

Data Availability Statement: All relevant data are within the manuscript and its Supporting Information files.

Funding: This research was supported by National Institutes of Health grant (DE013239) to RAB. The funders had no role in study design, data collection and analysis, decision to publish, or preparation of the manuscript.

Competing interests: The authors have declared that no competing interests exist.

Abstract

A recent genome-wide screen identified ~300 essential or growth-supporting genes in the dental caries pathogen *Streptococcus mutans*. To be able to study these genes, we built a CRISPR interference tool around the Cas9 nuclease (Cas9_{S_{mu}}) encoded in the *S. mutans* UA159 genome. Using a xylose-inducible dead Cas9_{S_{mu}} with a constitutively active single-guide RNA (sgRNA), we observed titratable repression of GFP fluorescence that compared favorably to that of *Streptococcus pyogenes* dCas9 (Cas9_{S_{py}}). We then investigated sgRNA specificity and proto-spacer adjacent motif (PAM) requirements. Interference by sgRNAs did not occur with double or triple base-pair mutations, or if single base-pair mutations were in the 3' end of the sgRNA. Bioinformatic analysis of >450 *S. mutans* genomes allied with *in vivo* assays revealed a similar PAM recognition sequence as Cas9_{S_{py}}. Next, we created a comprehensive library of sgRNA plasmids that were directed at essential and growth-supporting genes. We discovered growth defects for 77% of the CRISPRi strains expressing sgRNAs. Phenotypes of CRISPRi strains, across several biological pathways, were assessed using fluorescence microscopy. A variety of cell structure anomalies were observed, including segregational instability of the chromosome, enlarged cells, and ovo-cocci-to-rod shape transitions. CRISPRi was also employed to observe how silencing of cell wall glycopolysaccharide biosynthesis (rhamnose-glucose polysaccharide, RGP) affected both cell division and pathogenesis in a wax worm model. The CRISPRi tool and sgRNA library are valuable resources for characterizing essential genes in *S. mutans*, some of which could prove to be promising therapeutic targets.

Author summary

Streptococcus species cause diverse infections in humans including pneumonia and meningitis. They are common inhabitants of the mouth and certain species are associated with the incredibly prevalent oral disease dental caries (tooth decay). *Streptococcus mutans* is the most studied and most often linked organism to the development and progression of dental caries. Recent studies have shown that the genome of this organism encodes a

number of essential genes that are required for the survival of the bacteria. Many of these genes are conserved in other pathogenic streptococci, and some are unique to *S. mutans*. To facilitate the study of these genes in a high-throughput manner we developed a CRISPR interference gene-silencing system. This tool, which modifies the CRISPR-Cas9 system encoded by *S. mutans*, allowed us to study virtually all the essential genes encoded by the organism. We found that these genes are required for optimal growth of the organism. We also found that the morphological defects of these strains are diverse but also shared among genes related to similar molecular pathways. We used the CRISPRi tool to comprehensively assess the contribution of L-rhamnose glycopolymers to *S. mutans* viability, pathogenicity and coordination of cell division. Overall, these findings increase our understanding of *Streptococcus* essential genes, and may help in the development of new antimicrobial therapies.

Introduction

Streptococcus species are natural inhabitants of humans and animals. Under the right conditions many streptococci can cause or exacerbate diverse infections in humans, including life-threatening illnesses that include meningitis or pneumonia [1]. The transition between commensalism and pathogenicity is an important feature of the oral streptococci, which is the most abundant bacterial genus in the human mouth [2]. Oral streptococci have important roles in the initiation and maturation of dental biofilms (plaque), and many are associated with oral and dental health. However, oral streptococci that are especially acidogenic and acid-tolerant are implicated as primary etiologic agents in the pathogenesis of dental caries (tooth decay) [3]. Dental caries is a common cause of pain, impaired quality of life, and tooth loss in children and adults [3]. The organism most often linked to caries development is *Streptococcus mutans*, which has been shown to have multiple virulence traits, some unique, that imbue the organism with the capacity to initiate and worsen the disease [4]. Extraorally, *S. mutans* and other oral streptococci can cause infective endocarditis [5]. More recently, epidemiologic and mechanistic studies point to a role for certain *S. mutans* strains in cardiovascular diseases, including stroke [6]. Investigating the biology of this organism is important for developing therapies that combat dental caries and other diseases associated with *S. mutans* and related organisms. More broadly, expanding the understanding of streptococcal biology will positively impact efforts to prevent or treat many other diseases in humans and animals.

Antimicrobial therapies usually target biological processes that are essential for bacterial growth and persistence. These pathways include protein synthesis, transcription, DNA replication, cell division, peptidoglycan biosynthesis, or folic acid metabolism. The most traditional approach for discovering new antibiotics has been screening the ability of natural and synthetic compounds to inhibit growth or processes essential for pathogenesis [7]. Alternatively, antibacterial targets could be identified by combining genome sequence data with genome-wide techniques that probe gene essentiality, followed by the identification or design of molecules that target the factors involved in the process of interest [8]. Global identification of essential genes is possible with a technique known as transposon sequencing (Tn-seq) [9]. Using Tn-seq, we identified a panel of genes that are essential for the growth of *S. mutans* UA159, together with genes that are required for growth *in vitro* in rich or defined medium [10]. Although Tn-seq can be used to discover essential genes, it does not yield conditional mutations, and therefore does not allow for the functional study of these genes unless culture conditions can be found that allow for growth. Before moving toward studies that attempt to block or inhibit these pathways in *S. mutans*, or other streptococci, there is a need for further

validation and investigation of these apparently essential genes. However, functional studies of essential genes in bacteria have traditionally been technically challenging and time-consuming, because mutants of these genes cannot be isolated and studied. One approach involves the generation of a conditional knockout, usually by mutating an essential gene and simultaneously expressing a copy of the gene under the control of a promoter that can be activated by an exogenously provided compound [11]. Two major drawbacks to this approach are that it is not easily adapted to a comprehensive study of the essential genome of an organism in a time-efficient manner (low throughput) and differences in gene expression levels between the conditional expresser and the wild type can generate misleading results.

Reprogramming of the bacterial CRISPR (clustered regularly interspaced short palindromic repeats)-Cas system into a gene-silencing tool has made it more practical to perform high-throughput studies of essential genes [12,13]. This technique, known as CRISPR interference (CRISPRi), combines an inducible, catalytically inactive *Streptococcus pyogenes* Cas9 nuclease, dead Cas9 (dCas9), with a programmable single-guide RNA (sgRNA). The sgRNA encodes a 20-nt sequence that is complementary to the target DNA. When expressed together in a cell, the sgRNA-dCas9_{Spy} complex represses transcription initiation or elongation of the target gene. CRISPRi libraries that silence all putatively essential genes have been generated for both *Streptococcus pneumoniae* D39 [14] and *Bacillus subtilis* 168 [15]. A complicating factor for developing a CRISPRi system in *S. mutans* UA159 is the presence of an endogenous Cas9 nuclease (SMu.1405c) [16]. Introduction of a CRISPRi system into *S. mutans* built around dCas9_{Spy} would likely not function without the deletion of the endogenous Cas9, because of the potential for Cas9_{Smu}-sgRNA complexes to cause lethal double-strand breaks in the chromosome. It is known that Cas9_{Smu} and Cas9_{Spy} can cleave DNA in the presence of a *S. pyogenes* dual-RNA, and vice versa [17]. The Cas9 target recognition sequence, known as the protospacer adjacent motif (PAM), is also predicted to be 5'-NGG'-3' in *S. mutans*, as is the case in *S. pyogenes* [18]. Given the similarities, one possible approach to CRISPRi in *S. mutans* could be to repurpose the endogenous Cas9_{Smu} nuclease into a nuclease-dead version, while also using elements of the original interference system (e.g. sgRNA). A CRISPRi system built around Cas9_{Smu} could function more effectively in *S. mutans* than one based on Cas9_{Spy}. Heterologous expression of *S. pyogenes* dCas9 can be toxic to certain bacteria [19,20], although problems of this nature were not observed in a recent CRISPRi study in *S. pneumoniae* [14]. Irrespective of *S. pyogenes* dCas9 toxicity, the dCas9_{Spy} could perform suboptimally compared to dCas9_{Smu} simply due to codon-bias. Lastly, developing an *S. mutans* CRISPRi system has the potential to add to the number of tools for genome editing that are currently available.

Motivated by a desire to functionally study essential genes in *S. mutans*, we created a CRISPRi tool assembled around dCas9_{Smu}. We explored sgRNA specificity and PAM requirements, and compared interference activity with dCas9_{Spy}. Having demonstrated good CRISPRi activity, we then constructed a library of sgRNAs against all putative essential and growth-supporting genes [10]. With this library we evaluated growth and certain phenotypes in a subset of strains with CRISPRi-silenced essential genes. Finally, we used the technique to systematically study the impact that depletion of L-rhamnose-containing cell wall polysaccharides has on cell division and pathogenicity in an insect model.

Results

Robust gene knockdown with a titratable dCas9_{Smu} system

More than 95% of the 477 *S. mutans* strains for which whole or draft genome sequences are presently available carry at least one CRISPR-Cas system (Fig 1A). The Type II-A CRISPR-Cas system, which can be repurposed for CRISPRi, is the most prevalent across the species with

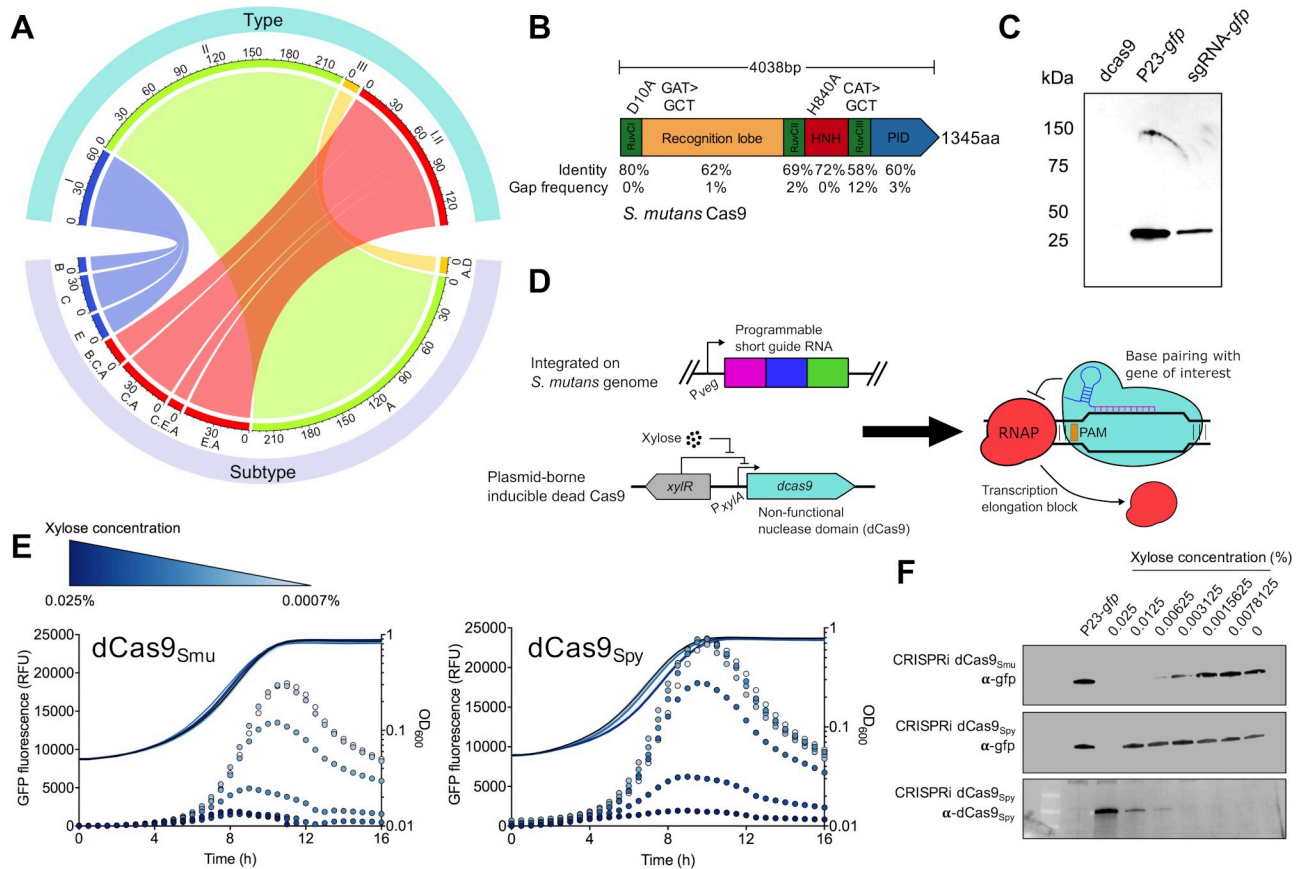


Fig 1. Design of an inducible CRISPRi gene-silencing system for *S. mutans*. (A) Distribution of CRISPR-Cas systems in *S. mutans* by type (top half) and subtype (bottom half). For example, 67 *S. mutans* strains contain Type I systems (blue), and the subtypes of this system are B, C, and E (I-C is the most common). The numbers on the exterior of the plot denote the number of *S. mutans* strains that possess a certain CRISPR-Cas system. (B) Diagram of the Cas9 protein of *S. mutans* UA159 showing domains. The two conserved amino acids required for nuclease activity in the *S. pyogenes* Cas9 protein that were mutated to create the *S. mutans* dCas9 protein are indicated. Each domain was compared with *S. pyogenes* Cas9 for percentage amino acid identity. (C) Gene-silencing activity of endogenous dCas9_{Smu} was assessed by expressing an sgRNA with complementarity to a chromosomally integrated *gfp* gene and comparing GFP protein levels using Western blotting (sgRNA-*gfp*). Also shown is a negative control, *dcas9* without *gfp*, and a positive control strain that constitutively expresses the *gfp* gene from the P23 promoter (see text for details). (D) Overview of the CRISPRi system engineered for *S. mutans*, which consists of two primary elements, a chromosomally located sgRNA and a plasmid-borne inducible dead Cas9. Combined, these two elements can block gene transcription as shown on the right. (E) Comparison of dCas9_{Smu} (left) and dCas9_{Spy} (right) *gfp* gene silencing activity using real-time fluorescence monitoring. Fluorescence readings are shown as dots, and cell density (OD₆₀₀) readings as lines. As the xylose concentration was decreased, data points change from a dark to a light blue color. (F) Comparison of dCas9_{Smu} (top panel) and dCas9_{Spy} (middle panel) *gfp* gene silencing activity with Western blotting as a function of xylose concentration. The bottom panel is a Western blot against the xylose-inducible dCas9_{Spy}; as this antibody detected dCas9_{Spy}, but not dCas9_{Smu}. Western images are representative of three independent replicates.

<https://doi.org/10.1371/journal.ppat.1008344.g001>

339/477 strains carrying a complete system (Fig 1A). For reprogramming of *S. mutans* UA159 Cas9 (SMu.1405c) into a CRISPRi system, we began by mutating two amino acid residues (D10 and H840) known to be required for the nuclease activity of *S. pyogenes* Cas9 [21] (Fig 1B). We were able to confirm the DNA-binding and repressing activity of dCas9_{Smu} by expressing a sgRNA against a constitutively expressed *gfp* gene [22] (Fig 1C). Next, the *S. mutans* *dcas9* gene was cloned into pZX9 [23], such that expression could be activated by xylose. Prior to this, we discovered, using green fluorescent protein (GFP) as a readout for xylose-induced gene expression, that the P_{xyI} promoter was less active when glucose was the sole carbohydrate source compared to maltose (S1 Fig in S1 File). We suspect the different expression levels on glucose versus maltose could be due to carbohydrate catabolite repression and/or effects of certain phosphoenolpyruvate:sugar phosphotransferase system (PTS)

components on P_{xyl} activity. Thus, we used the defined media ‘FMC’ containing maltose for all CRISPRi related experiments. To make the CRISPRi strain (Fig 1D), the sgRNA plasmid was integrated in single copy into the *S. mutans* genome in a strain that contained i) a *gfp* gene driven by the constitutively active P23 promoter and integrated into the chromosome, ii) the P_{xyl} -*dcas9*_{Smu} plasmid and iii) point mutations that prevent translation of SMU.1405c (*cas9*; start codon mutated to stop codon). *S. mutans* Cas9 must be mutated, otherwise endogenous *cas9* expression in combination with sgRNAs would likely cause lethal chromosome damage; *S. mutans* is unable to repair the double-strand cleavage catalyzed by a functional Cas9.

Having developed the system, we moved to assessing its efficiency. Using the *S. mutans* CRISPRi technique, we observed titratable repression of GFP fluorescence (Fig 1E) and GFP protein levels (Fig 1F). Importantly, there were no obvious effects on the growth of *S. mutans* as increasing amounts of xylose were added (up to 0.025% w/v). Also of note, slightly higher amounts of xylose (0.025% vs. 0.00625%) were required to achieve similar levels of repression of GFP production in a strain containing a xylose-inducible *S. pyogenes dcas9* (Fig 1E and 1F). We also observed slight growth impairments as increasing amounts of dCas9_{Spy} were produced (Fig 1E). Overall, the differences in performance of the two Cas9 constructs were minor. Next, we measured gene-silencing (absence of GFP fluorescence) at the single-cell level (S2 Fig in S1 File). The number of cells escaping CRISPRi-mediated gene knockdown (GFP positive) was very small, indicating that, at saturating amounts of xylose, the effects of the *S. mutans*-derived CRISPRi system are uniform across the population when the dCas9 protein is delivered on a multi-copy plasmid. The pZX9 plasmid that carries the xylose-inducible system uses the streptococcal replicon from pDL278. Without antibiotic pressure we have shown that pDL278 is stable in *S. mutans* for at least 50 generations [22].

RNA sequencing (RNA-seq) experiments were conducted to test the effects of the CRISPRi system on the *S. mutans* transcriptome. We compared the transcriptome of the CRISPRi strain without and with the addition of xylose (0.1%). With xylose, we observed an increase in dCas9 expression and a concomitant decrease in *gfp* expression compared to the no xylose condition (S1 Table). This was specific to the presence of sgRNA-*gfp* as we observed no reduction in *gfp* expression in a strain lacking the sgRNA and xylose added (no sgRNA in S1 Table). As has been noted by other authors [13,14] we measured a polar effect of CRISPRi on genes downstream of the target gene (*msmK* and *dexB* are downstream of the location of the *gfp* gene). Importantly, the effect of CRISPRi induction on the *S. mutans* transcriptome was minimal. We observed no *S. mutans* gene expression changes with a $\log_2FC > 2$, and only twelve genes with a $\log_2FC > 1$ (FDR < 0.05). Furthermore, these twelve genes typically contained low read counts, indicating that the slight changes in gene expression could be attributable to noise. In the absence of CRISPRi, but with xylose (no sgRNA strain), no changes in *S. mutans* gene expression were observed; so 0.1% xylose has no discernable impact on the *S. mutans* transcriptome. From these RNA-seq results, we conclude that the CRISPRi system is highly specific and does not appreciably alter *S. mutans* gene expression other than targeted genes.

Guide RNA design principles for the sgRNA-Cas9_{Smu} system

To begin to optimize the *S. mutans* CRISPRi system, we examined parameters that are important for functionality; the first of these was sgRNA specificity. sgRNA-Cas9 systems that operate with lower sequence stringency could be prone to off-target effects that occur when guide RNA and dCas9 bind to a site(s) in the genome that was not intended to be affected. To test this, we cloned an sgRNA with a complementary sequence for the gene *atpB*, which encodes the beta subunit of the F₁F₀ proton-translocating ATPase. We modified the sgRNA-*atpB* sequence by introducing substitutions along the length of guide RNA (Fig 2A). The sgRNA

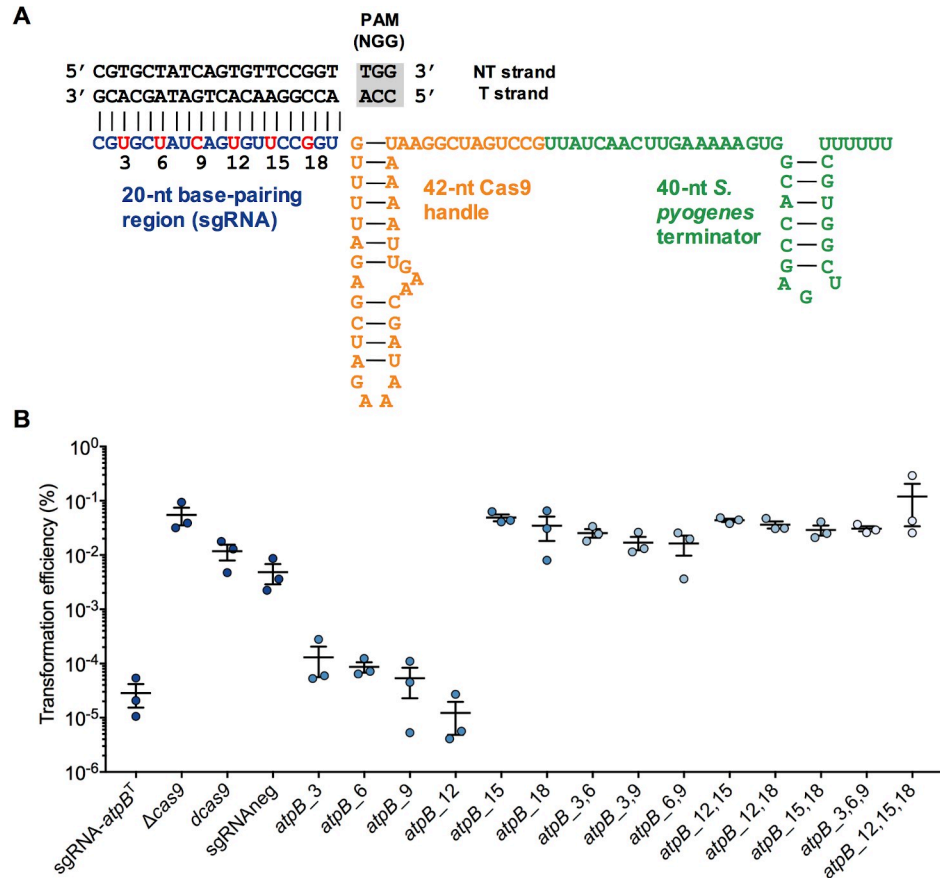


Fig 2. Determining guide RNA specificity of Cas9_{smu}. (A) Diagram of the sgRNA for *atpB* and the mutagenesis strategy. Positions 3, 6, 9, 12, 15 and 18 of the sgRNA were mutated (including in pairs or triplets) as a way of investigating sgRNA specificity (see text for additional details). (B) Plasmid interference assay of wild-type and mutated sgRNA-*atpB* plasmids, with Δ*cas9*, *dcas9* and sgRNAneg serving as controls (for no plasmid interference). If the plasmid interfered with *S. mutans atpB* expression, a lower transformation efficiency would be expected.

<https://doi.org/10.1371/journal.ppat.1008344.g002>

plasmids were added to competent *S. mutans* and plated onto selective agar. We expected that transformation into *S. mutans* of the sgRNA-*atpB* plasmid lacking sequence modifications would not be tolerated, leading to a very low transformation efficiency. As expected, transformation of the sgRNA-*atpB*^T (T; targeting the template strand) occurred at very low efficiency, 1 x 10⁻⁵ (Fig 2B). Conversely, transformation efficiency in a Δ*cas9* (deletion of Smu.1405c) strain, the dead *cas9* strain, or in a strain carrying a deletion of 20-bp of the *atpB*^T sequence from the sgRNA (sgRNAneg) was 100- to 1000-fold more efficient than with the intact *atpB* sgRNA (Fig 2B).

We next evaluated the effects of expressing sgRNAs with one, two or three base mutations within the *atpB*^T sequence. Single base-pair mismatches were tolerated at the 5' end of the sgRNA (*atpB*_3, *atpB*_6, *atpB*_9 and *atpB*_12). Plasmids with mismatches closer to the PAM (*atpB*_15 and *atpB*_18) transformed with higher efficiency into *S. mutans*, indicative of a loss of sgRNA activity. All of the double and triple base mismatches reduced the activity of the sgRNAs, as these plasmids transformed *S. mutans* at levels comparable to the *cas9*-deficient strain (Fig 2B). These results suggest that near perfect sgRNA sequence complementarity is required to silence genes, and thus it should be possible to minimize off-target effects with careful design of sgRNAs.

Another important feature of CRISPR-Cas9 systems, both as a natural bacterial immune system and for CRISPRi, is the proto-spacer adjacent motif (PAM). This sequence is required for the Cas9 protein to recognize interference targets and is also critical during the acquisition of CRISPR spacers (for Type II-A systems) [21,24]. For a given bacterial strain, Type II-A PAM sequences are generated by aligning CRISPR spacers to phage genomes, extracting the sequence downstream of the spacer target, and then building a conserved sequence from these. The difficulty with taking this approach with *S. mutans* UA159 is that there are too few CRISPR spacers from which to build a reliable PAM sequence. Consequently, we compiled PAM sequences from a large (>450) collection of *S. mutans* genomes. After narrowing the data to strains that had Type II-A CRISPR-Cas systems and ≥ 5 spacers, PAM sequences were generated for 100 individual *S. mutans* strains using WebLogo (S3 Fig in S1 File). Per this bioinformatics analysis, a highly conserved PAM for Cas9_{Smu} was not evident. Rather, a significant number of *S. mutans* strains with Cas9 contained spacers that might require the 5'-NGG-3' recognition sequence for phage DNA interference, and these spacer arrays grouped together by alignment (Fig 3A, yellow color). For other *S. mutans* strains with Cas9, PAM sequences were more random, but at least two other groups, 5'-TTN-3' and 5'-NAAA-3', existed (S3 Fig in S1 File). We observed no obvious grouping for *S. mutans* of the predicted PAM sequences by Cas9 protein identity (Fig 3A). We reasoned that PAM recognition might be protein sequence specific and thus expected that the different PAM groups predicted by bioinformatics would also group together. A lack of coherence between the predicted PAM sequences and Cas9 protein sequences suggests that the PAM sequences assembled via bioinformatics may not be the best indicator of the requirements for recognition for all *S. mutans* strains. So, to investigate DNA recognition in greater detail we developed an interference assay with GFP fluorescence as the readout. Using site-directed mutagenesis we incorporated assorted PAMs into a construct in which the P23 promoter could drive the expression of a *gfp* gene (Fig 3B). This assay confirmed that *S. mutans* dCas9 recognizes a 5'-NGG-3' PAM (Fig 3C). With 5'-NAG-3' we observed moderate CRISPRi activity with dCas9_{Smu}, although the results varied as a function of the DNA base present in the first position, with up to an 80% loss of GFP fluorescence. Weak binding of *S. pyogenes* Cas9 to a 5'-NAG-3' PAM has been reported before [25–27]. Nuclease activity via 5'-NGA-3' recognition has previously been reported for Cas9_{Spy} [26,27] but we were unable to observe CRISPRi activity with either dCas9 protein with a 5'-AGA-3' PAM. No interference was observed with any of the other PAM sequence combinations tested.

Creation of a comprehensive library of essential gene targeting sgRNAs

We constructed a library of sgRNAs targeting 253 potentially essential and growth supporting genes (Fig 4A). These genes (S2 Table) were selected from previously conducted Tn-seq experiments [10], Tn-seq performed as part of this study, and genes shown to be essential in previous studies (e.g. *vicR/walR*). We were unable to design sgRNAs for 21 putative essential or growth supporting genes, of which over half (12) were ribosomal proteins. These genes were small (average size of 275-bp) and generally lacked PAM sites that would give desirable sgRNA sequences (e.g. RNA folding, off-target effects, location in 5' region of gene). During the first round of cloning (see Materials and Methods) we obtained correct sgRNA clones for 181 of 282 (64%) of the desired strains. After three rounds of cloning 259/282 (92%) of the sgRNAs were successfully cloned. We were unable to obtain sgRNA clones for 23 (8%) genes. After plasmid cloning in *E. coli* 10-beta, sequence-verified sgRNA plasmids were transformed into *S. mutans* $\Delta cas9$ P_{xyt}-dCas9_{Smu}. While it would be possible to clone the sgRNA plasmids directly into *S. mutans*, we wanted to minimize the number of passages in *S. mutans* as CRISPRi strains are known to acquire suppressors when guide RNAs are expressed in their hosts [14].

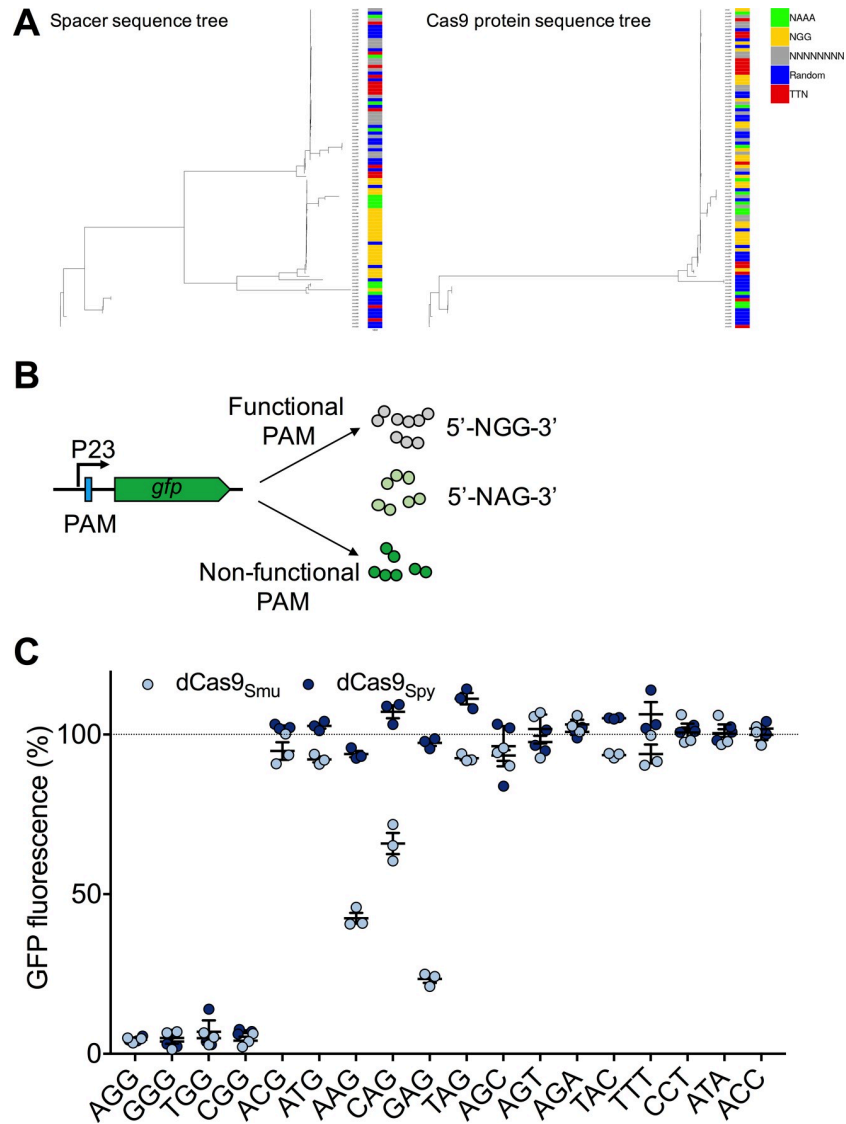


Fig 3. Investigating the proto-spacer adjacent motif (PAM) requirements of Cas9_{Smu}. (A) Phylogenetic relatedness of extracted CRISPR-Cas9 spacer sequences (left) and Cas9 protein sequences (right). Consensus PAM sequences were built from spacer sequences and are available in S3 Fig in [S1 File](#). A key describing the colors chosen for consensus PAM sequences is shown on the far right. (B) To determine the optimal PAM sequence for dCas9_{Smu}, different PAM sequences were inserted into between the P23 promoter and *gfp* gene. (C) The functionality of various PAM sequences were compared by measuring CRISPRi repression of GFP fluorescence for both *S. pyogenes* and *S. mutans* Cas9. Repression was calculated as a percentage of maximal fluorescence without exogenous xylose compared to fluorescence with 0.1% xylose added. Bars show the average and standard deviation, and light blue dots are the individual values, obtained using the dCas9_{Smu} construct, whereas the dark blue dots show data obtained using dCas9_{Spy}. Maximal repression was measured with a 5'-NGG-3' PAM, with moderate repression for some 5'-NAG-3' PAMs.

<https://doi.org/10.1371/journal.ppat.1008344.g003>

Growth phenotypes of strains with silenced essential genes

We measured the growth of each sgRNA strain in FMC-maltose either in the absence or presence of 0.1% xylose for 16 h using a Bioscreen C Automated Microbiology Growth Curve System. Afterwards, the area under the curve (AUC) was calculated for both conditions. Quantification of growth by AUC is useful as it combines growth phases (lag, exponential and

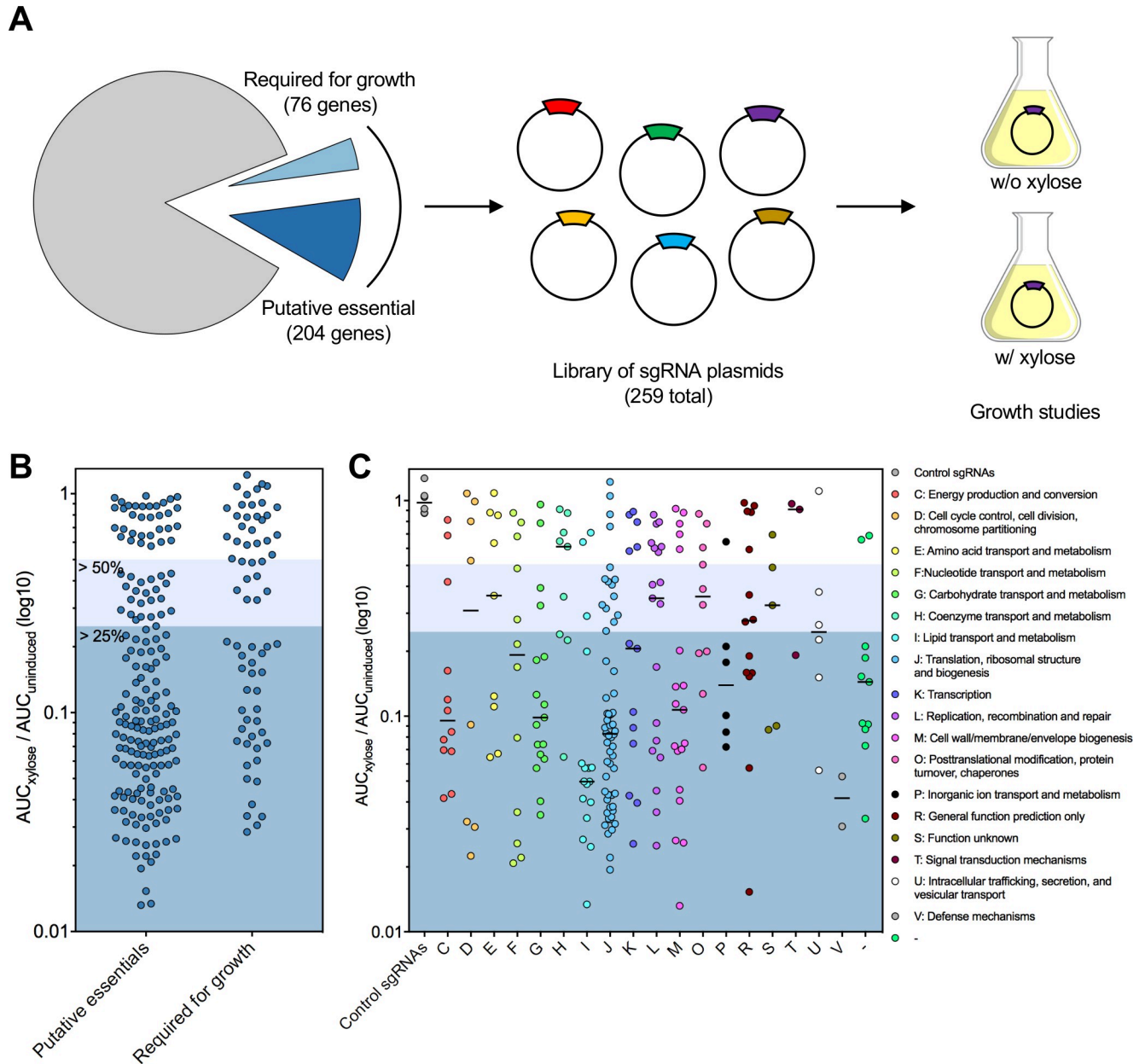


Fig 4. High-throughput growth analysis of a comprehensive library of sgRNAs targeting essential and growth supporting genes. (A) Overview of the CRISPRi growth study that included generating sgRNAs against >250 essential or growth-supporting genes. Growth analysis of CRISPRi strains (B) whether putative essential or required for growth and (C) sorted for physiological functions by Clusters of Orthologous Groups. CRISPRi strains were cultured in the presence or absence of xylose and the area under the curve (AUC) was calculated for each condition. Growth phenotypes were categorized according to the ratio of AUC_{xylose} to $AUC_{uninduced}$ (the lower the number the stronger the growth defect).

<https://doi.org/10.1371/journal.ppat.1008344.g004>

stationary phases). For each strain, the AUC_{xylose} was divided by $AUC_{uninduced}$. Growth phenotypes were grouped per these ratios: >0.5, minor phenotype; 0.25–0.49, moderate growth defect; <0.25, strong growth defect. It is important to note that the differences between strains slightly above or below the ratio cut-off points are not substantial. Growth defects were observed in 194/253 (77%) of the strains expressing sgRNAs that were designed to target essential or growth supporting genes (Fig 4B; S2 Table). Overall, we observed a higher percentage of growth defects for strains with silenced essential genes versus growth-supporting genes, 82%

and 62%, respectively (Fig 4B). When comparing between different Clusters of Orthologous Groups (COGs), the two lowest median growth defects were observed for silenced genes in the translation (J) and lipid metabolism and transport pathways (I) (Fig 4C; silenced genes in the category defense mechanisms (V) displayed strong growth defects but we are unsure of these genes functions). The two highest median growth defects were observed when sgRNAs targeted genes related to coenzyme transport and metabolism (H) and signal transduction mechanisms (T) (Fig 4C). Growth defects were not observed for the six sgRNAs that targeted non-essential genes (*scrB*, *lacG*, *gtfB*, *bceA*, *gfp*, *gfpprom*; see S2 Table). There was no significant relationship between the growth defect we observed and the position of the sgRNA within the gene or the size of the target gene (S4 Fig in S1 File).

Assessing cell biology phenotypes of CRISPRi strains with microscopy

Next we evaluated the morphological phenotypes of eighty CRISPRi strains placed in the following functional categories: fatty acid biosynthesis/membrane biogenesis, peptidoglycan synthesis, glycolysis, DNA replication, transcription, translation, cell division, and ATP synthase activity. Using DAPI staining, we were able to visualize the bacterial chromosome, and with Nile red we could detect the cell membrane. The cell morphology defects of essential gene-targeted strains were diverse (Fig 5). Defects included increased cell chaining, abnormally large cells, heterogeneously sized cells, cell lysis and anucleate cells (S5-S12 Figs in S1 File). The most commonly observed morphological phenotypes across all the pathways investigated were increased cell chaining (e.g. *pfk*, *accD*, *dnaE*, *rs3*, *atpC*) and heterogeneously sized cells (e.g. *pgi*, *glmM*, *dnaG*, *eftS*, *atpF*) (Fig 5A). It is important to note that there were strains without obvious growth defects that displayed major cell morphology defects (e.g. *ftsX* and *glmS*). Repression of genes involved in the glycolysis pathway led to significant growth defects and larger/misshapen cells (S5 Fig in S1 File). When *pgm*, encoding phosphoglucomutase, was repressed, cells appeared to be somewhat rod-shaped, probably associated with altered or deficient biosynthesis of cell wall polysaccharides. When genes involved in peptidoglycan biosynthesis were repressed, the most common phenotype was the formation of singular large round cells (S6 Fig in S1 File). The percentage of cells displaying this phenotype varied, with it being most common in a strain with silenced *murM*, which in *S. pneumoniae* encodes a protein that incorporates amino acids into the side-chain of peptidoglycan [28]. Repression of genes involved in the conversion of acetyl-CoA to malonyl-CoA (*accACD* and *bccP*), an important step in fatty acid biosynthesis, led to excessive chaining of cells (S7 Fig in S1 File). Repression of fatty acid biosynthetic (*fab*) genes yielded minor phenotypic changes, whereas silencing of genes downstream of the FAS II pathway (*plsX* and *cdsA*) led to more obvious morphological defects. As anticipated, when genes involved in DNA replication were repressed, not all cells contained nucleoids (S8 Fig in S1 File). In addition to anucleate cells, certain CRISPRi strains with repressed chromosome replication also showed severe morphological defects (e.g. *dnaE*, *dnaG*, *priA*). CRISPRi repression of translation-related genes increased cell chaining (S9 Fig in S1 File). When the ribosomal proteins *rs3* (small ribosomal subunit) and *r111* (large ribosomal subunit) were repressed, we observed anucleate cells that lacked a well-defined cell envelope. CRISPRi silencing of genes encoding subunits of the F₁F₀-ATPase led to strong growth defects, increased cell chaining and variability in Nile red staining (S10 Fig in S1 File). Repression of transcription-related genes also led to increased cell chaining and attenuated growth (S11 Fig in S1 File). The cell shape and size of *rpoB*-, *rpoC*-, and *rpoZ*-silenced CRISPRi strains were severely impacted. When genes involved in cell division were repressed, strains displayed heterogeneity in cell size and shape (S12 Fig in S1 File). Notably, with repression of *divIC*, *ftsA*, *ftsL* and *ftsZ* we observed similar morphological changes. Cells appeared to be rod-shaped,

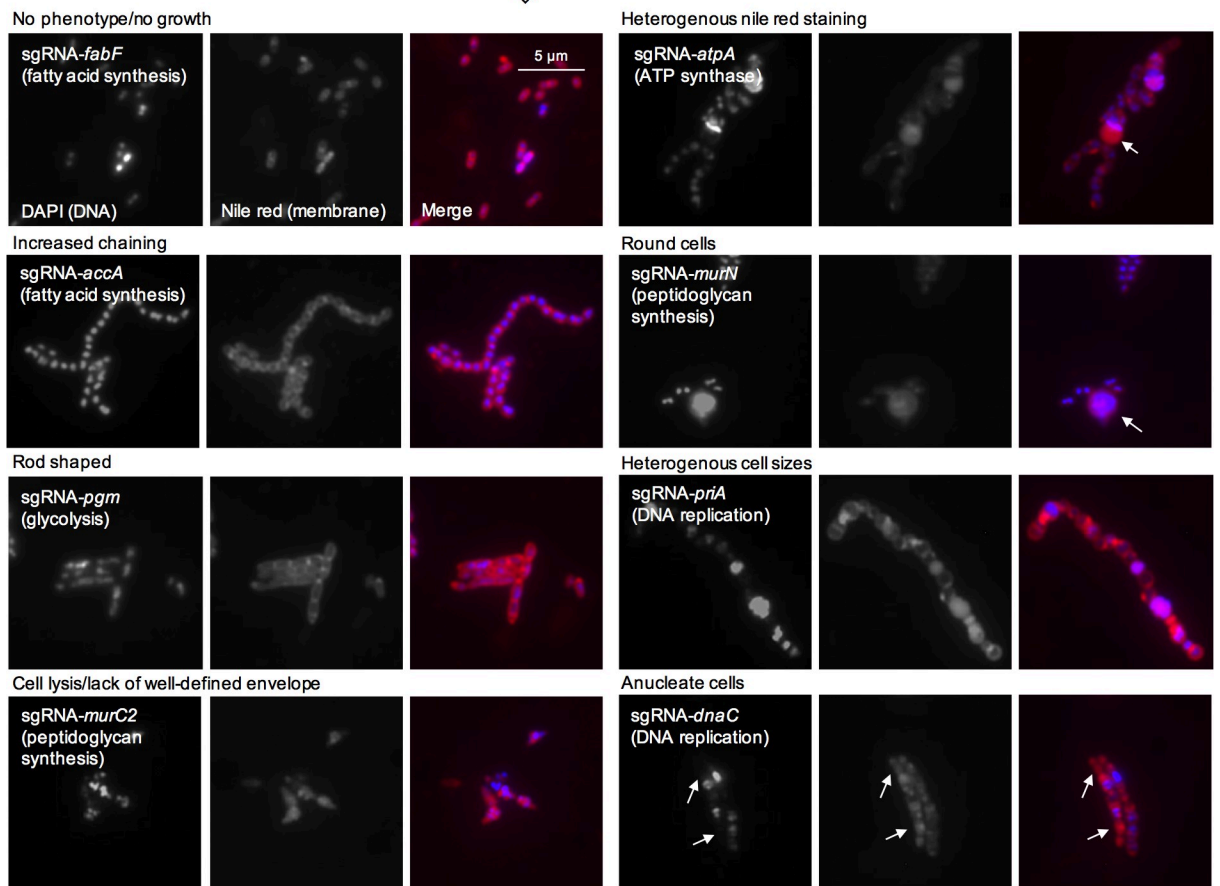
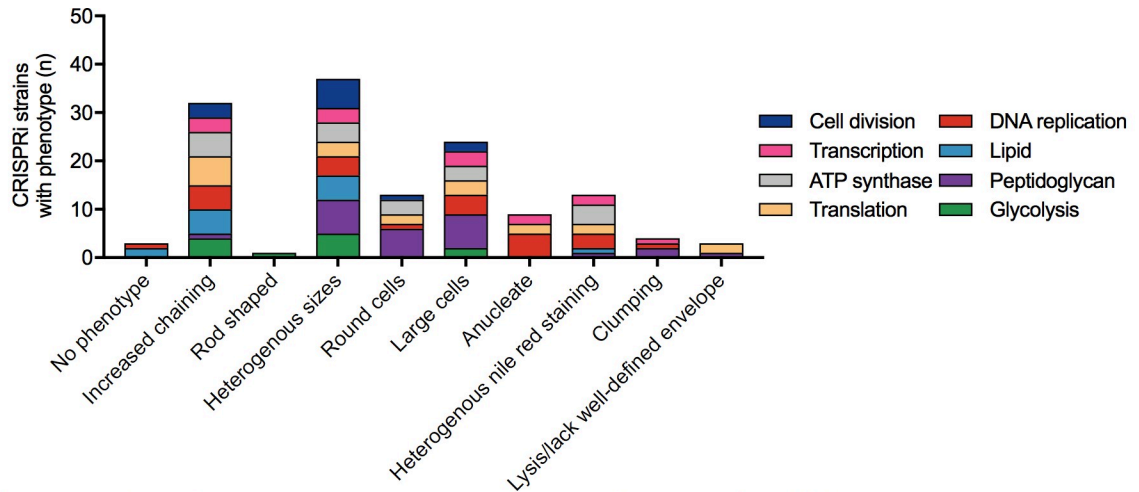


Fig 5. Microscopic analysis of the morphological defects caused by CRISPRi essential gene depletion. (A) CRISPRi strains, by functional pathway, were grouped according to cell morphology phenotypes. Strains with depleted essential genes can have more than one morphological defect (e.g. increased cell chaining and heterogeneous sizes). (B) Representative micrographs for several of the cell morphology phenotypes that were observed are shown. Additional microscopy across all the pathways investigated can be found in S5–S12 Figs in [S1 File](#). For *sgRNA-atpA* the arrow shows an area of increased Nile red staining compared to other cells. The large round cells observed when silencing peptidoglycan biosynthesis is depicted with the *sgRNA-murN* micrograph. Arrows indicate potential anucleate cells when targeting the DNA replication-related gene *dnaC*.

<https://doi.org/10.1371/journal.ppat.1008344.g005>

except that they bulged at the cell septum, probably consistent with an inability of these cells to complete septation. FtsZ is a tubulin homologue that forms a Z-ring at the midcell that is important for scaffolding and cytokinesis [29]. FtsA, DivIC and FtsL also localize to the mid-cell (at different stages) during cell division [29]. Repression of *gpbB* (glucan-binding protein B), an ortholog of the *S. pneumoniae* peptidoglycan hydrolase gene, *pcsB*, led to cell division defects. Although specific peptidoglycan hydrolase activity has not been observed for GbpB, the cell division defects we observed, along with the observation that GbpB can be localized to areas of active peptidoglycan synthesis [30], provide support for the idea that it may act enzymatically to affect the structure of the cell wall. Taken together, microscopic analysis of CRISPRi strains from different pathways has revealed generalized phenotypes of essential gene depletion, but also clear functional links between genes in established pathways.

Identification of GpsB (SMu.471) as a critical cell division determinant of *S. mutans*

Next we wanted to employ CRISPRi as a tool to study poorly annotated essential genes in *S. mutans*. The gene SMu.471 and the intergenic region downstream of it were of interest to us as we noticed that this region did not tolerate transposon insertions (Fig 6A). After conducting BLASTn analysis of the intergenic region, we realized that the RNA component of RNase P, *rnpB*, is located here. The *rnpB* transcript, as measured by RNA-seq, was highly abundant, which is consistent with what has been observed in other bacteria [31]. RNase P is a ribonucleoprotein that catalyzes the maturation of the 5' end of pre-tRNAs [32]. To characterize the gene SMu.471, we began with CRISPRi phenotyping, which showed that depletion leads to a strong growth defect (Fig 6B). Depletion of SMu.471 also led to cell morphology defects (Fig 6D). Cells were wider and larger than wild-type and some appeared to not be correctly dividing (Fig 6D). Although annotated as a hypothetical protein, BLASTp analysis showed that

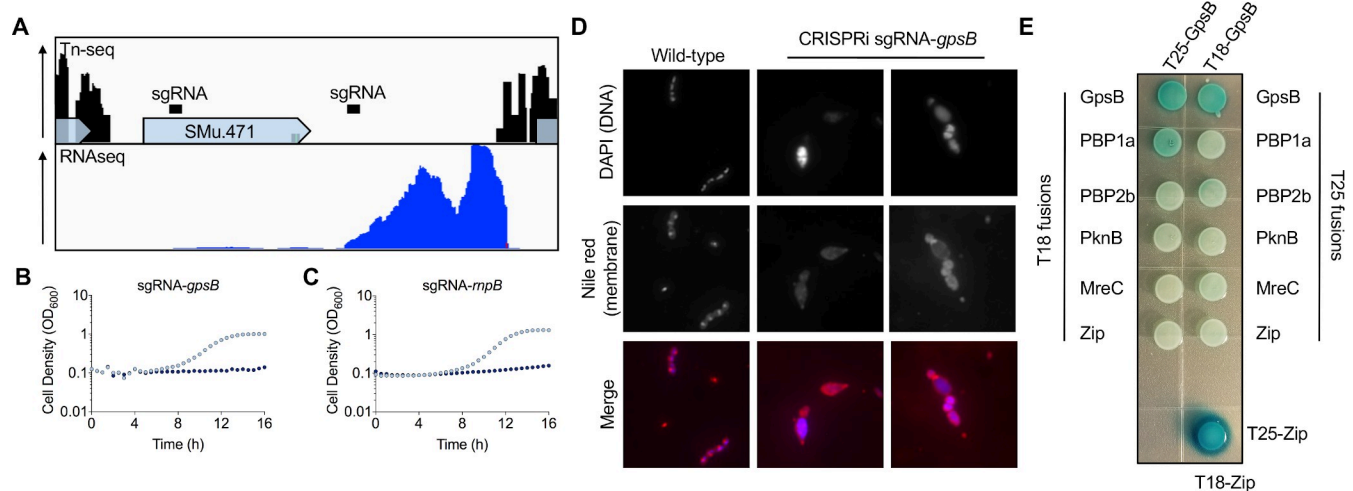


Fig 6. Identification of the essential peptidoglycan synthesis regulator GpsB in *S. mutans*. (A) Distribution of Tn-seq reads (top panel) within SMu.471 and the downstream intergenic region. Each peak corresponds to a transposon insertion with a lack of peaks within a gene representative of an essential gene (e.g. SMu.471). RNA sequencing reads (bottom panel) obtained from mid-log *S. mutans* cells grown in FMC-maltose. High levels of transcription are evident in the region downstream of SMu.471, which is likely to be the RNA component of RNase P (*rnpB*). CRISPRi growth phenotypes of silenced *gpsB* (SMu.471; B) and *rnpB* (C). Strains were cultured in FMC-maltose without (light blue dots) or with (dark blue dots) 0.1% xylose. (D) Microscopic analysis of a CRISPRi strain with depleted levels of *gpsB*. Strains were cultured overnight in FMC-maltose containing 0.1% xylose, stained with DNA and membrane staining dyes, and then imaged with fluorescence microscopy. Images are representative of five independent replicates. (E) Bacterial two-hybrid screening to test interactions between GpsB and putative interaction partners. Interactions were tested using constructs cloned into two plasmids pKT25 and pUT18C (T18 and T25 fusions). A positive control is shown on the bottom right (T25-zip with T18-zip). GpsB interacts with itself and has a weak interaction with PBP1a as shown by blue colonies (β -galactosidase activity has been restored by interactions between the two proteins; see S1 File for a description of the methodology).

<https://doi.org/10.1371/journal.ppat.1008344.g006>

SMu.471 contains a GpsB/DivIVA domain. SMu.471 aligned best with GpsB proteins from other Gram-positive organisms (S14 Fig in [S1 File](#)), consistent with it being smaller (112 aa) than true DivIVA proteins. Of note, the *S. mutans* UA159 genome contains three proteins with DivIVA domains, SMu.471, SMu.557, and SMu.1260c (S14 Fig in [S1 File](#)). SMu.557 (271 aa) is larger than SMu.471, whereas SMu.1260c is the smallest protein of the three (59 aa) (S14 Fig in [S1 File](#)). GpsB proteins are smaller than DivIVA proteins because of a reduction in the length of the C-terminal domain (CTD). GpsB has been shown to interact with a diverse assortment of proteins involved in cell division, with penicillin-binding protein (PBP) interactions (predominately class A) being most common [33]. We tested the interaction of GpsB with PBPs, as well as with the cell elongation protein MreC [34–36], or the serine/threonine protein kinase PknB [34], using a bacterial-two-hybrid assay. We observed self-interaction of GpsB and a weak interaction with PBP1a, but no interaction was evident for either MreC or PknB (Fig 6E). Collectively, the CRISPRi growth defect, cell morphology changes and the interaction with PBP1a suggest that GpsB is a critical cell division protein in *S. mutans*.

L-rhamnose glycopolymers are critical for *S. mutans* cell division and pathogenicity

Having shown that CRISPRi allows for the functional study of essential genes, we next focused our attention on a pathway that is thought to be of major importance to *S. mutans*, rhamnose-glucose polysaccharide (RGP) biosynthesis. Certain streptococcal species lack cell wall teichoic acids (WTAs) and instead produce RGPs that are covalently linked to the peptidoglycan [37]. RGP biosynthesis begins with a four-step pathway encoded by the genes *rmlABCD* that converts glucose-1-phosphate into dTDP-L-rhamnose. The last gene in the pathway, *rmlD*, resides in an operon (SMu.824-835) that contains genes required for additional RGP biosynthesis steps and transport of the carbohydrates through the cell membrane. By our Tn-seq analysis, most of the genes involved in producing RGP are either essential or required for the growth of *S. mutans* UA159 (Fig 7A) [10]. L-rhamnose biosynthetic pathways are also essential in *S. pyogenes* [38] and *Mycobacterium smegmatis* [39]. Several of these genes have, however, been mutated in *S. mutans*, including *rmlBC* [40], *rmlD* [38], *rgpE* [30,41], *rgpF* [41,42], and *rgpG* [43]. Inconsistencies between our observations and others could be related to the nature of our Tn-seq selection and/or the presence of undetected suppressor mutations that bypass essentiality in strains that carry RGP gene deletions in other studies. Use of CRISPRi to study RGP function facilitates the rapid evaluation of depleting each gene product under conditions that allow for selective pressure to be applied only when xylose is provided in the medium. By CRISPRi, down-regulation of every gene directly involved in RGP biosynthesis displayed severe growth defects when silenced with sgRNAs (Fig 7B; S13 Fig in [S1 File](#)). In the invertebrate infection model organism *Galleria mellonella*, strains with silenced *rmlB*, *rgpC*, and *rgpF* genes displayed attenuated virulence compared to wild-type *S. mutans* UA159 and a *dcas9* strain (Fig 7C). For this proof-of-concept study, sgRNAs were expressed in an *S. mutans* strain where the endogenous Cas9 had been converted to dCas9. Using this approach, no xylose is required and instead genes are repressed by the constitutively produced dCas9 (Fig 1C). A strain with silenced *rmlD* was not attenuated. However, we suspect this strain acquired suppressor mutation(s) as it originally grew very poorly, but after some passage it was able to grow to a final OD₆₀₀ similar to the parental strain. Having shown that RGP biosynthesis genes are required for growth in laboratory media and during infection, we next investigated their importance to *S. mutans* cell biology. Consistent with previous observations [30,43], cellular morphologies were exceptionally aberrant, compared to the wild type (S13 Fig in [S1 File](#)). Cells were large, not consistently ovococoid, and formed longer chains than normal.

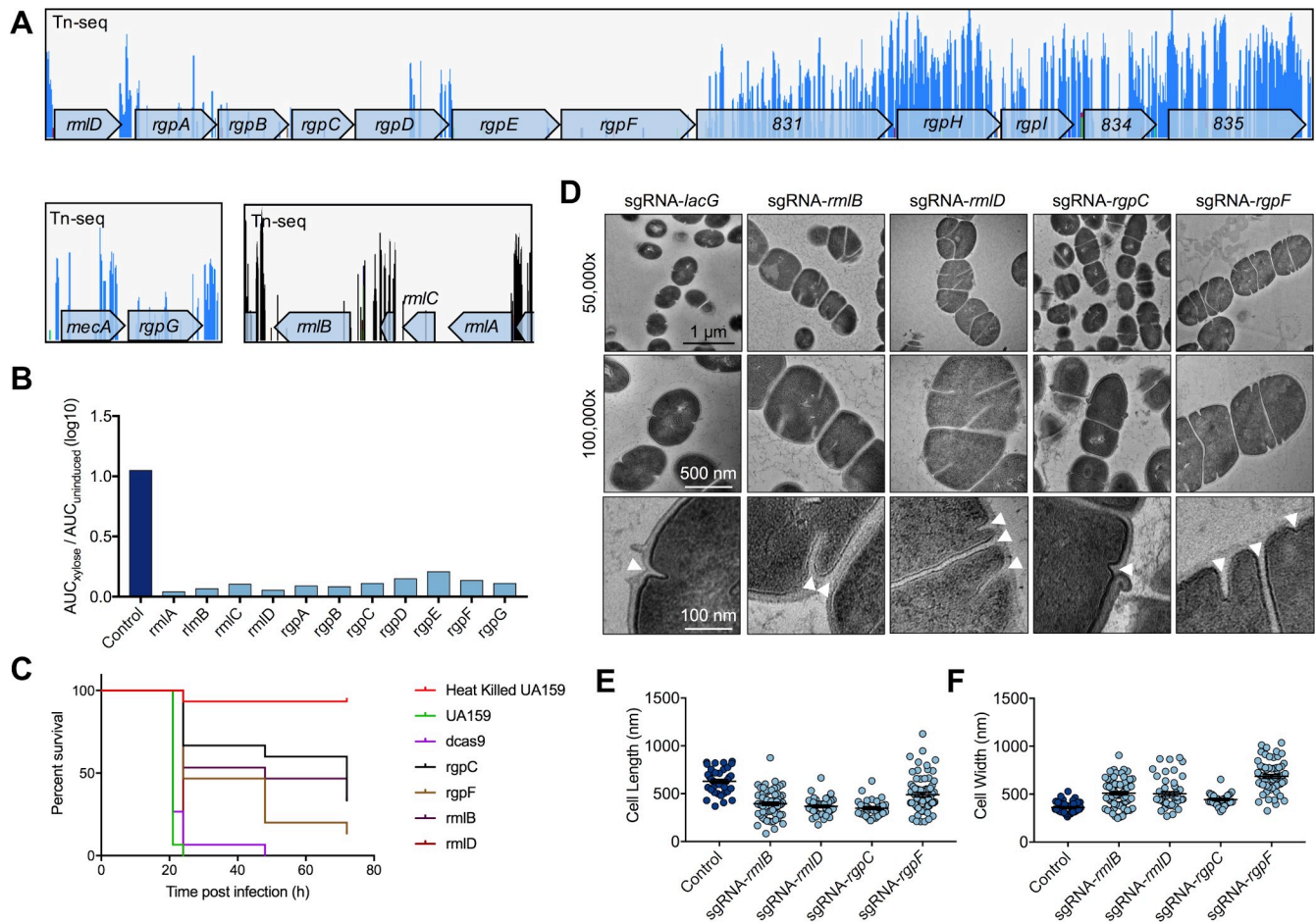


Fig 7. Rhamnose-glucose polysaccharide biosynthesis genes are required for growth, pathogenesis and correct cell division of *S. mutans*. (A) Distribution of Tn-seq reads within genes that function in RGP biosynthesis (*rmlA-rmlC*, *rgpG*, and *rmlD-rgpF*; SMu.831-835 reside in the operon that starts with *rmlD*). Each peak corresponds to a transposon insertion with a lack of peaks within a gene representative of an essential gene (e.g. *rmlA* or *rgpE*). (B) Growth phenotypes of silenced RGP biosynthesis genes compared to a control strain (*sgRNA-lacG*). (C) Pathogenesis phenotypes of silenced RGP biosynthesis genes (*rmlB*, *rmlD*, *rgpC*, and *rgpF*) in a *Galleria mellonella* infection model. Heat killed UA159 served as a negative control, and wild-type UA159 and *dcas9* absent *sgRNA* as positive controls. (D) Electron micrographs of CRISPRi strains targeting the same genes investigated in the pathogenesis model. Arrowheads point to putative division septa. Fluorescence microscopy images and growth curves for CRISPRi strains for all of the genes involved in this pathway can be found in S13 Fig in S1 File. Cell length (E) and width (F) measurements from TEM micrographs using ImageJ.

<https://doi.org/10.1371/journal.ppat.1008344.g007>

Although resolutions were limiting, it also appeared that certain large cells contained multiple nucleoids by DAPI strain (S15 Fig in S1 File). To gain greater ultrastructural insights, we investigated cell biology phenotypes of *rmlB*, *rmlD*, *rgpC*, and *rgpF* silenced strains with transmission electron microscopy (TEM). In these strains, division site positioning was irregular and not always in the mid-point of cells (Fig 7D). There were instances where the division septum was unable to traverse the cell (*rmlB*, *rmlD*, *rgpF*) or cells had double septa (*rgpF*) (Fig 7D). Accordingly, large cells with incomplete septation appeared to have multiple unequally sized compartments, which likely has a deleterious effect on chromosome segregation, and might explain the unusual patterns of DAPI staining observed during fluorescence microscopy (S15 Fig in S1 File). In *rgpC*-silenced cells, the equatorial ring, an outgrowth of cell wall material that is normally duplicated and separates as cells divide, was abnormally thick and in some cases was 'peeling' back from the cell (Fig 7D). Measurements from the CRISPRi strain micrographs using ImageJ confirmed that they were wider than wild-type cells (Fig 7E).

Discussion

Essential genes represent promising targets for antimicrobials. The essential genome of *S. mutans* is comprised of ~300 genes and, like other bacteria, is enriched for genes that function in processing genetic information, energy production, and maintenance of the cell envelope. However, until the recent development of CRISPRi technologies, high-throughput functional studies of these genes has not been possible. Here we demonstrate the conversion of the *S. mutans* Cas9 nuclease into a gene silencing tool for the systematic interrogation of the essential genome. Our system is relatively streamlined as it only requires a constitutively expressed sgRNA and a xylose-inducible dCas9. Importantly, it allowed us to study all the known essential genes in a relatively short time. Most of the genes predicted to be essential by Tn-seq displayed strong growth defects once silenced by CRISPRi. Furthermore, CRISPRi strains with sgRNAs targeting essential genes displayed morphological defects when analyzed by microscopy. This work confirms the importance of these genes to the integrity of *S. mutans* cells, and of their potential as interesting therapeutic targets for the control of *S. mutans* or certain other pathogenic streptococci.

One interesting finding of this work is that Cas9_{S_{mu}} recognition of target DNA shares similarities with Cas9_{S_{py}}. First, guide RNA specificity of Cas9_{S_{mu}} is similar to Cas9_{S_{py}} as single base-pair mismatches are not tolerated in the 5' region of sgRNA (the seed region) [44,45]. Cas9_{S_{mu}} was also unable to cause DNA cleavage *in vivo* when double or triple base-pair mutations were introduced into the sgRNA sequence, again consistent with findings in Cas9_{S_{py}} [45]. Second, PAM recognition relied on a 5'-NGG-3' sequence. We also observed moderate CRISPRi activity with a 5'-NAG-3' PAM. Cas9_{S_{py}} activity also relies on a 5'-NGG-3' PAM with weak DNA recognition reported for the non-canonical PAMs 5'-NAG-3' and 5'-NGA-3' [25–27], although we were unable to measure this with our assay. Although target recognition also relies on other factors [46], we are confident that off-target effects should be minimized when using a 5'-NGG-3' PAM and a guide RNA designed to ensure a lack of complementarity (two or more mismatches) to other regions of the genome. The similarities of Cas9_{S_{mu}} and Cas9_{S_{py}} are interesting given that other streptococcal Cas9 nucleases require PAMs that differ to 5'-NGG-3' [20,47]. For example, the Cas9 of *Streptococcus canis*, which shares ~90% sequence similarity to Cas9_{S_{py}}, recognizes a 5'-NNG-3' PAM [47]. Bioinformatics analysis of the species-wide PAM requirements were cryptic, but it is possible that other *S. mutans* Cas9 proteins recognize alternative PAMs *e.g.* 5'-NAAA-3'. Intriguingly the Cas9 of *Streptococcus macacae* NCTC 11558 is presumed to recognize an adenine enriched PAM [48]. There is an arms race between the bacteria that generate Cas9 proteins recognizing new PAMs and the phage that undergo mutations to avoid CRISPR interference, with the latter being a confounding issue with PAMs that are generated solely using bioinformatic tools. Despite these limitations, it is possible there is species-wide PAM diversity, similar to what has been observed with *Neisseria meningitidis* [49]. This is an interesting area of study as it should aid in the engineering of new variants of Cas9 that recognize different PAMs, thus expanding the genetic engineering capabilities of the Cas9 proteins.

The CRISPRi system described here was able to perturb the expression of over 250 putative essential and growth-supporting genes. The severe growth defects exhibited by most of these strains emphasizes their critical functions in *S. mutans*. The percentage of silenced genes that displayed significant growth defects was comparable with what was observed for *S. pneumoniae* [14]. As noted above, CRISPRi has many advantages over more traditional approaches for studying essential genes, but the technique has its limitations. For example, failure to display an aberrant growth phenotype could be caused by sub-optimal sgRNA design or selection for suppressor mutations that bypass essentiality. Likewise, certain essential genes could still

function with a low number of protein molecules per cell if the target gene is not completely silenced. In some cases, strains that displayed relatively minor growth defects when the target genes were depleted had significant alterations in cell morphology. Tn-seq, which was used to identify candidate genes for this study [10], is a competitive assay, so even mutants with minor growth phenotypes could be significantly underrepresented at the chosen end-point. In this study, we supplemented our previous Tn-seq essential gene analysis [10] with a different Tn-seq approach, which involved plating the original library on BHI instead of blood agar, then passaging the libraries in BHI or FMC for ~10 generations, as compared with ~30 generations in our previous study [10]. The differences between the older and the newer Tn-seq analysis were minor (S2 Table). Overall, the CRISPRi growth study paired with comprehensive Tn-seq enquiries provide a solid foundation for determining which genes are essential in *S. mutans* UA159. It is reasonable to predict that some of these gene products could be targeted for the therapeutic control of *S. mutans* and possibly some other pathogenic streptococci.

In addition to growth studies, we were able to observe morphological phenotypes of CRISPRi strains with light and electron microscopy. Several morphology phenotypes were evident that were consistent with other high-throughput microscopic studies of essential gene depletions [14,15]. The changes in morphology could represent more generalized responses to an inability to grow or, in some cases, may prove useful in linking gene products that function in concert. For example, *ftsA*, *ftsZ*, *ftsL* and *divIC* shared similar phenotypes, consistent with their products being required for correct cell septum formation. Perturbation of peptidoglycan synthesis led in some cases to the formation of large round cells. Blocking or deleting peptidoglycan synthesis genes in other bacteria can lead to the generation of giant cells [50] or L-forms [51], although the phenotypes in this study appear distinct from those previously described variants.

The rhamnose-glucose polysaccharide (RGP) of mutans streptococci were used in the past to differentiate serotypes of strains that were previously all designated as *S. mutans*. Today, it is recognized that the species *S. mutans* consists primarily of Bratthall serotypes *c*, *e*, and *f*, along with the unusual serotype *k* strains [52,53]. In contrast, what was formerly designated serotype *b* *S. mutans* is now classified as *Streptococcus rattii*. It is also now well recognized that RGP is an important constituent of the envelope of mutans streptococci. Clear impacts on growth, pathogenicity and cell division were observed in strains that had silenced genes contributing to RGP biogenesis. The cell morphology phenotypes were stark, with depletion strains clearly exhibiting aberrant septum formation, as has been noted before in *S. mutans* and other related species [30,54,55]. An inability to divide normally has been linked to aberrant localization of the peptidoglycan hydrolase PcsB (GbpB in *S. mutans*) [30,55]. When *gbpB* was targeted with CRISPRi, cells appeared to be unable to divide correctly (S12 Fig in S1 File), but the phenotype did not match that associated with *rgp* gene silencing. Given the vital role and essentiality of the RGP biosynthetic pathway, coupled with the decreased virulence of certain *rgp* knock-downs reported here, RGP biogenesis may be an attractive antimicrobial target. Further, if RGP and peptidoglycan synthesis are linked, it is conceivable that targeting RGP biosynthesis could potentiate the efficacy of β -lactam and other cell wall-active antibiotics. Other attractive aspects of the RGP pathway as an antimicrobial target include the species or strain-specificity of the glycopolymers and the absence of the pathway in humans [37].

In summary, this is the first study to utilize CRISPRi in *S. mutans* as a genetic tool. We did so by repurposing the Cas9 that is widely distributed among the species, opening new avenues for investigating the diversity of CRISPR-Cas in *S. mutans* and other oral streptococci, and the possible development of next-generation CRISPR-Cas tools. We demonstrate that the technique provides a powerful approach for studying essential genes and gene function, in agreement with studies using other organisms [14,15]. We anticipate that these tools can be used to

investigate new aspects of *S. mutans* cell biology and to identify promising therapeutic candidates.

Materials and Methods

Bacterial strains and growth conditions

Strains of *Streptococcus mutans* were cultured in Brain Heart Infusion (BHI) broth (Difco) or chemically defined medium (FMC) [56] supplemented with 0.5% maltose. Streptococci were grown in a 5% CO₂ aerobic environment at 37°C, unless stated otherwise. Strains of *Escherichia coli* were routinely grown in lysogeny broth (LB) with slight modifications (Lennox LB; 10 g/L tryptone, 5 g/L yeast extract and 5 g/L NaCl) at 37°C with aeration. Antibiotics were added to growth media at the following concentrations: kanamycin (1.0 mg/ml for *S. mutans*, 50 µg/ml for *E. coli*), erythromycin (10 µg/ml for *S. mutans*, 300 µg/ml for *E. coli*), spectinomycin (1.0 mg/ml for *S. mutans*, 50 µg/ml for *E. coli*) and ampicillin (100 µg/ml for *E. coli*). Strains and plasmids are listed in [S3 Table](#).

CRISPR-Cas bioinformatics

The 477 *S. mutans* genomes available in the National Center for Biotechnology Information (NCBI) GenBank in June 2018 were mined using CRISPRone [57] to determine the occurrence and diversity of CRISPR-Cas systems in this species. CRISPR arrays were also identified using CRISPRone and these were used to predict the PAM sequence based on spacer-protospacer matches using CRISPRtarget [58]. Afterwards, consensus PAM sequences for each strain were built using the WebLogo server [59].

Construction of the xylose-inducible CRISPRi system

Xylose-inducible plasmids were cloned by following a protocol developed by Xie *et al* [23]. Three plasmids were generated that contained *gfp*, *dcas9_{S_{mu}}* and *dcas9_{S_{py}}* inserts cloned into the pZX9 plasmid. For each plasmid, two linear fragments were created by PCR using pZX9 or *S. mutans* UA159 genomic DNA as templates. *dcas9_{S_{py}}* was amplified from a plasmid obtained from Addgene (Addgene #44249). *dcas9_{S_{mu}}* was amplified from the strain described in the supplemental material. The *gfp* gene was amplified from previously constructed *gfp*-reporter strains [22]. The PCR fragments are designed so that they have overlapping complementary regions that facilitate concatemer formation during a 2nd PCR. The products generated by this 2nd PCR are transformed directly into *S. mutans*. Primers pZX9seqF and pZX9seqR were used to amplify gene inserts followed by Sanger sequencing. For cloning of the sgRNA plasmid (pPM::sgRNA), a synthetic DNA fragment was generated (Integrated DNA Technologies) that contained the following components sequentially: 1) a P_{veg} promoter [22], 2) a 20-nt sgRNA targeting *gfp*, 3) a 42-nt dCas9 binding handle sequence, and 4) an *S. pyogenes* terminator. Restriction enzyme recognition sequences for *SacI* and *SphI* were included at the 5' and 3' ends of the sgRNA construct respectively. The synthetic DNA fragment was subsequently cloned into the pPMZ plasmid which integrates at the *phnA-mtIA* locus of *S. mutans* UA159. This plasmid was also used to generate plasmids containing sgRNAs that target other areas of the *S. mutans* genome. Protocols for cloning of additional strains are provided in [S1 File](#). Oligonucleotides used in this study are listed in [S4 Table](#).

Green fluorescent protein CRISPRi assay

To test the CRISPRi system and compare the activity of dCas9_{S_{mu}} to dCas9_{S_{py}} we used a GFP based assay. CRISPRi strains were cultured overnight, grown to an OD₆₀₀ = 0.5, and then

diluted 1:100 into FMC-maltose with or without xylose. For these assays the concentration of xylose was serially diluted. In triplicates, 200 μ L samples were added to clear-bottomed, black-sided, 96-well microtiter plates. After loading of the cultures, the 96-well plate was placed in a Synergy HT microtiter plate reader (BioTek). The fluorescence and optical density (absorbance at 600 nm) were measured at 30-min intervals using Gen5 software (BioTek). The fluorescence settings were excitation at 485 nm, emission at 525 nm, and a sensitivity of 65. Data readings were collected, and the background fluorescence or OD₆₀₀ was subtracted prior to data visualization using GraphPad Prism (v7) software (GraphPad Software). A slightly modified version of this assay was used for PAM comparisons (S1 File). The protocol for Western blotting of GFP and dCas9_{spy} is available in S1 File.

sgRNA library design and cloning

sgRNA sequences (20-nt) were selected with CRISPy-web [60]. With this tool we uploaded the *S. mutans* UA159 GenBank file (NC_004350.2) and selected essential genes. For each gene, the tool designs sgRNAs with predicted off-target matches (13-bp upstream of the PAM; off-targets containing 0, 1, 2, or 3-bp mismatches). To minimize off-target effects we only selected sgRNAs with two or more mismatches, which we have shown to diminish sgRNA activity (Fig 2B). We also aimed to select sgRNA sequences as close to the start of each gene as possible. For each sgRNA we predicted the secondary structure (20-nt sequence and 42-nt dCas9 binding handle) with the RNAfold program provided by ViennaRNA [61]. Only sgRNAs that maintained the hairpin structure of the dCas9 binding handle were selected for cloning. sgRNA sequences were cloned using the Q5 Site-Directed Mutagenesis Kit (New England Biolabs). Primers were designed using the NEBaseChanger tool (v.1.2.9), substituting the sgRNA-*gfp* 20-nt sequence for whichever sgRNA we were cloning. Using the designed primers, the pPM::sgRNA plasmid was amplified and then added to a mix of Kinase-Ligase-*DpnI* for 5 min at room temperature. This mixture (5 μ L) was then transformed into chemically competent *E. coli* 10-beta with selection on LB-kanamycin. For each sgRNA plasmid transformation, two independent clones were selected and cultured overnight. With each culture we made a glycerol stock for storage at -80°C, and purified plasmid with the QIAprep Spin Miniprep Kit (Qiagen). Each plasmid was Sanger sequenced using the pRCS1seqR primer (S4 Table).

sgRNA plasmid interference assays

sgRNA sequence specificity was tested using a plasmid interference assay. A 20-nt sequence complementary to the template strand of the *atpB* gene (SMu.1528) was introduced into the pPM::sgRNA plasmid with the Q5 Site-Directed Mutagenesis Kit. Using the same kit, single, double, or triple base-pair mismatches were introduced into the 20-nt *atpB* sgRNA sequence. These plasmids were transformed into competent *S. mutans* and cells were serially diluted onto BHI agar, or BHI agar containing kanamycin. The percentage of cells that were transformed was calculated from the colony forming units present on both types of agar.

CRISPRi growth assays

Strains of *S. mutans* carrying sgRNA cassettes were grown overnight in BHI with the appropriate antibiotics in a microaerophilic environment at 37°C. The following day the bacterial cultures were washed once in FMC-maltose, and then diluted 1:1000 into FMC-maltose or FMC-maltose containing 0.025% xylose. Triplicates of 300 μ L were added to a Bioscreen C 10 x 10 well plate for each condition. OD₆₀₀ was measured every 30 min for 16 h with a Bioscreen C Automated Microbiology Growth Curve Analysis System (Growth Curves USA).

Fluorescence microscopy of CRISPRi strains

Overnight cultures of CRISPRi strains were diluted 1:100 into 200 μ L FMC-maltose containing 0.025% xylose, and then incubated at 37°C in a 5% CO₂ incubator for 16 h. After incubation, 1 μ L of 1 mg/mL Nile red (ThermoFisher Scientific) was added to each sample and incubated for 5 min at room temperature (RT) in darkness. Next, 1 μ L of 1 mg/mL DAPI (4',6-diamidino-2-phenylindole; ThermoFisher Scientific) was added to each sample and incubated at RT in darkness for a further 5 min. Samples were centrifuged for 5 min at 4,000 x g and suspended in ProLong Live Antifade Reagent (ThermoFisher Scientific). For imaging, 2.5 μ L of stained cells were placed on PBS (pH 7.4; 137 mM NaCl, 2.7 mM KCl, 8 mM Na₂HPO₄, 2 mM KH₂PO₄) agarose pads [62] before sealing with a coverslip. Images were captured with a Zeiss Axiovert 200M microscope equipped with a Zeiss AxioCam MRm camera using a 100X oil objective.

Transmission electron microscopy

CRISPRi strains were grown as described for fluorescence microscopy. Afterwards cells were rinsed with 0.1M sodium cacodylate buffer and then fixed in 3% glutaraldehyde overnight at 4°C. The following day, cells were treated with 1.5% osmium tetroxide in the dark for 1 h at 4°C. Next the cells were mixed in equal parts with 5% agarose in PBS, collected by centrifugation at 2000 x g, and cooled to 4°C. Small chunks of the bacterial pellet plus agarose were then dehydrated in ethanol via the following steps: 30%, 50%, 70%, 80%, 90% each for 15 min, 99% 10 min, and then absolute ethanol 2 x 10 min. The dehydrated cells were embedded in an epoxy resin, sectioned and stained with uranyl acetate and lead citrate. Microscopy was conducted using a Hitachi H7600 transmission electron microscope.

Waxworm experiments

Galleria mellonella killing assays were performed as described previously [63]. Insects in the final instar larval stage were purchased from Vanderhorst, Inc. (St. Marys, OH), stored at 4°C in the dark and used within 7 days of shipment. Groups of 15 larvae, ranging in weight from 200 to 300 mg and with no signs of melanization, were selected at random for subsequent infection. Insects were injected with 1x10⁷ CFU of bacterial inoculum, prepared from overnight cultures that had been washed and resuspended in 0.9% saline solution, into the hemocoel of each larva via the last left proleg using a 25- μ L Hamilton syringe. Fifteen larvae were injected for each condition. The number of viable cells injected into the larvae was verified by colony counts on BHI plates. As a negative control, one group of *G. mellonella* were injected with UA159 that was heat killed at 80°C for 30 minutes. After injection, insects were kept at 37°C and survival at different time intervals was recorded. Larvae were scored as dead when thigmotaxis was absent. Kaplan-Meier killing curves were plotted, and estimations of differences in survival were compared using a log rank test. All data were analyzed with GraphPad Prism, version 7.0c software. Experiments were repeated three times.

Supporting information

S1 File Supplemental text. This document includes supplemental materials and methods and S1 to S15 Figs. (DOCX)

S1 Table. Transcriptomic changes measured by RNA-seq in CRISPRi strains. This file contains read counts and data analysis examining transcriptomic changes that occur when the

CRISPRi system is induced in *S. mutans*.
(XLSX)

S2 Table. CRISPRi Database. This file contains all data relating to CRISPRi gene-silencing of putative essential and growth supporting genes.
(XLSX)

S3 Table. Strains and plasmids used in this study.
(XLSX)

S4 Table. Oligonucleotides used in this study.
(XLSX)

S5 Table. Raw data for figures.
(XLSX)

S6 Table. Raw data for supporting figures.
(XLSX)

S7 Table. Number of transposon reads per gene.
(XLSX)

Acknowledgments

We thank Dr. Sharon Matthews and Chao Chen at the Electron Microscopy core at the University of Florida for help with TEM imaging and analysis; Dr. Vincent Richards for sending us the *S. mutans* genomes; Dr. Justin Merritt for providing us with the pZX plasmids for xylose-inducible gene expression in *S. mutans*; Dr. Edward Chan and John Calise for use of, and technical assistance with, fluorescence microscopy; and Dr. Stephen Hagen for use of single-cell microscopic tools.

Author Contributions

Conceptualization: Robert C. Shields, Robert A. Burne.

Data curation: Robert C. Shields, Alejandro R. Walker, Natalie Maricic, Brinta Chakraborty, Simon A. M. Underhill.

Formal analysis: Robert C. Shields.

Funding acquisition: Robert A. Burne.

Investigation: Robert C. Shields.

Methodology: Robert C. Shields, Robert A. Burne.

Writing – original draft: Robert C. Shields, Robert A. Burne.

Writing – review & editing: Robert C. Shields, Alejandro R. Walker, Natalie Maricic, Simon A. M. Underhill, Robert A. Burne.

References

1. Krzyściak W, Pluskwa KK, Jurczak A, Kościelniak D. The pathogenicity of the *Streptococcus* genus. *Eur J Clin Microbiol Infect Dis*. 2013; 32: 1361–1376. <https://doi.org/10.1007/s10096-013-1914-9> PMID: 24141975
2. Dewhirst FE, Chen T, Izard J, Paster BJ, Tanner ACR, Yu W-H, et al. The human oral microbiome. *J Bacteriol*. 2010; 192: 5002–17. <https://doi.org/10.1128/JB.00542-10> PMID: 20656903

3. Pitts NB, Zero DT, Marsh PD, Ekstrand K, Weintraub JA, Ramos-Gomez F, et al. Dental caries. *Nat Rev Dis Primer*. 2017; 3: 17030. <https://doi.org/10.1038/nrdp.2017.30> PMID: 28540937
4. Lemos JA, Quivey RG, Koo H, Abranches J. *Streptococcus mutans*: a new Gram-positive paradigm? *Microbiology*. 2013; 159: 436–45. <https://doi.org/10.1099/mic.0.066134-0> PMID: 23393147
5. Nomura R, Nakano K, Nemoto H, Fujita K, Inagaki S, Takahashi T, et al. Isolation and characterization of *Streptococcus mutans* in heart valve and dental plaque specimens from a patient with infective endocarditis. *J Med Microbiol*. 2006; 55: 1135–1140. <https://doi.org/10.1099/jmm.0.46609-0> PMID: 16849735
6. Nakano K, Hokamura K, Taniguchi N, Wada K, Kudo C, Nomura R, et al. The collagen-binding protein of *Streptococcus mutans* is involved in haemorrhagic stroke. *Nat Commun*. 2011; 2: 485. <https://doi.org/10.1038/ncomms1491> PMID: 21952219
7. Lewis K. Platforms for antibiotic discovery. *Nat Rev Drug Discov*. 2013; 12: 371–387. <https://doi.org/10.1038/nrd3975> PMID: 23629505
8. Juhas M, Eberl L, Church GM. Essential genes as antimicrobial targets and cornerstones of synthetic biology. *Trends Biotechnol*. 2012; 30: 601–607. <https://doi.org/10.1016/j.tibtech.2012.08.002> PMID: 22951051
9. van Opijnen T, Bodi KL, Camilli A. Tn-seq: high-throughput parallel sequencing for fitness and genetic interaction studies in microorganisms. *Nat Methods*. 2009; 6: 767–72. <https://doi.org/10.1038/nmeth.1377> PMID: 19767758
10. Shields RC, Zeng L, Culp DJ, Burne RA. Genomewide Identification of Essential Genes and Fitness Determinants of *Streptococcus mutans* UA159. *mSphere*. 2018; 3: e00031–18. <https://doi.org/10.1128/mSphere.00031-18> PMID: 29435491
11. Fan F, Lunsford RD, Sylvester D, Fan J, Celesnik H, Iordanescu S, et al. Regulated Ectopic Expression and Allelic-Replacement Mutagenesis as a Method for Gene Essentiality Testing in *Staphylococcus aureus*. *Plasmid*. 2001; 46: 71–75. <https://doi.org/10.1006/plas.2001.1526> PMID: 11535039
12. Bikard D, Jiang W, Samai P, Hochschild A, Zhang F, Marraffini LA. Programmable repression and activation of bacterial gene expression using an engineered CRISPR-Cas system. *Nucleic Acids Res*. 2013; 41: 7429–7437. <https://doi.org/10.1093/nar/gkt520> PMID: 23761437
13. Qi LS, Larson MH, Gilbert LA, Doudna JA, Weissman JS, Arkin AP, et al. Repurposing CRISPR as an RNA-Guided Platform for Sequence-Specific Control of Gene Expression. *Cell*. 2013; 152: 1173–1183. <https://doi.org/10.1016/j.cell.2013.02.022> PMID: 23452860
14. Liu X, Gally C, Kjos M, Domenech A, Slager J, van Kessel SP, et al. High-throughput CRISPRi phenotyping identifies new essential genes in *Streptococcus pneumoniae*. *Mol Syst Biol*. 2017; 13: 931–931. <https://doi.org/10.15252/msb.20167449> PMID: 28490437
15. Peters JM, Colavin A, Shi H, Czarny TL, Larson MH, Wong S, et al. A Comprehensive, CRISPR-based Functional Analysis of Essential Genes in Bacteria. *Cell*. 2016; 165: 1493–1506. <https://doi.org/10.1016/j.cell.2016.05.003> PMID: 27238023
16. Serbanescu MA, Cordova M, Krastel K, Flick R, Beloglazova N, Latos A, et al. Role of the *Streptococcus mutans* CRISPR-Cas Systems in Immunity and Cell Physiology. *J Bacteriol*. 2015; 197: 749–761. <https://doi.org/10.1128/JB.02333-14> PMID: 25488301
17. Fonfara I, Le Rhun A, Chylinski K, Makarova KS, Lécrivain A-L, Bzdrenga J, et al. Phylogeny of Cas9 determines functional exchangeability of dual-RNA and Cas9 among orthologous type II CRISPR-Cas systems. *Nucleic Acids Res*. 2014; 42: 2577–2590. <https://doi.org/10.1093/nar/gkt1074> PMID: 24270795
18. van der Ploeg JR. Analysis of CRISPR in *Streptococcus mutans* suggests frequent occurrence of acquired immunity against infection by M102-like bacteriophages. *Microbiol Read Engl*. 2009; 155: 1966–1976. <https://doi.org/10.1099/mic.0.027508-0>
19. Cho S, Choe D, Lee E, Kim SC, Palsson B, Cho B-K. High-Level dCas9 Expression Induces Abnormal Cell Morphology in *Escherichia coli*. *ACS Synth Biol*. 2018; 7: 1085–1094. <https://doi.org/10.1021/acssynbio.7b00462> PMID: 29544049
20. Rock JM, Hopkins FF, Chavez A, Diallo M, Chase MR, Gerrick ER, et al. Programmable transcriptional repression in mycobacteria using an orthogonal CRISPR interference platform. *Nat Microbiol*. 2017; 2: 16274. <https://doi.org/10.1038/nmicrobiol.2016.274> PMID: 28165460
21. Jinek M, Chylinski K, Fonfara I, Hauer M, Doudna JA, Charpentier E. A Programmable Dual-RNA-Guided DNA Endonuclease in Adaptive Bacterial Immunity. *Science*. 2012; 337: 816–821. <https://doi.org/10.1126/science.1225829> PMID: 22745249
22. Shields RC, Kaspar JR, Lee K, Underhill SAM, Burne RA. Fluorescence tools adapted for real-time monitoring of the behaviors of *Streptococcus* species. *Appl Environ Microbiol*. 2019; 85: e00620–19. <https://doi.org/10.1128/AEM.00620-19> PMID: 31101614

23. Xie Z, Qi F, Merritt J. Development of a tunable wide-range gene induction system useful for the study of streptococcal toxin-antitoxin systems. *Appl Environ Microbiol*. 2013; 79: 6375–84. <https://doi.org/10.1128/AEM.02320-13> PMID: 23934493
24. Heler R, Samai P, Modell JW, Weiner C, Goldberg GW, Bikard D, et al. Cas9 specifies functional viral targets during CRISPR–Cas adaptation. *Nature*. 2015; 519: 199–202. <https://doi.org/10.1038/nature14245> PMID: 25707807
25. Leenay RT, Maksimchuk KR, Slotkowski RA, Agrawal RN, Gomaa AA, Briner AE, et al. Identifying and Visualizing Functional PAM Diversity across CRISPR–Cas Systems. *Mol Cell*. 2016; 62: 137–147. <https://doi.org/10.1016/j.molcel.2016.02.031> PMID: 27041224
26. Zhang Y, Ge X, Yang F, Zhang L, Zheng J, Tan X, et al. Comparison of non-canonical PAMs for CRISPR/Cas9-mediated DNA cleavage in human cells. *Sci Rep*. 2014; 4. <https://doi.org/10.1038/srep05405> PMID: 24956376
27. Kleinstiver BP, Prew MS, Tsai SQ, Topkar V, Nguyen NT, Zheng Z, et al. Engineered CRISPR–Cas9 nucleases with altered PAM specificities. *Nature*. 2015; 523: 481–485. <https://doi.org/10.1038/nature14592> PMID: 26098369
28. Filipe SR, Tomasz A. Inhibition of the expression of penicillin resistance in *Streptococcus pneumoniae* by inactivation of cell wall muropeptide branching genes. *Proc Natl Acad Sci U S A*. 2000; 97: 4891–4896. <https://doi.org/10.1073/pnas.080067697> PMID: 10759563
29. Massidda O, Nováková L, Vollmer W. From models to pathogens: how much have we learned about *Streptococcus pneumoniae* cell division? *Environ Microbiol*. 2013; 15: 3133–3157. <https://doi.org/10.1111/1462-2920.12189> PMID: 23848140
30. Kovacs CJ, Faustoferri RC, Bischer AP, Quivey RG. *Streptococcus mutans* requires mature rhamnose-glucose polysaccharides for proper pathophysiology, morphogenesis and cellular division. In: *Molecular Microbiology* [Internet]. 12 Jul 2019 [cited 14 Aug 2019]. <https://doi.org/10.1111/mmi.14330> PMID: 31210392
31. Chen Z, Itzek A, Malke H, Ferretti JJ, Kreth J. Multiple Roles of RNase Y in *Streptococcus pyogenes* mRNA Processing and Degradation. *J Bacteriol*. 2013; 195: 2585–2594. <https://doi.org/10.1128/JB.00097-13> PMID: 23543715
32. Kazantsev AV, Pace NR. Bacterial RNase P: a new view of an ancient enzyme. *Nat Rev Microbiol*. 2006; 4: 729–740. <https://doi.org/10.1038/nrmicro1491> PMID: 16980936
33. Halbedel S, Lewis RJ. Structural basis for interaction of DivIVA/GpsB proteins with their ligands. *Mol Microbiol*. 2019; 111: 1404–1415. <https://doi.org/10.1111/mmi.14244> PMID: 30887576
34. Rued BE, Zheng JJ, Mura A, Tsui H-CT, Boersma MJ, Mazny JL, et al. Suppression and Synthetic-Lethal Genetic Relationships of Δ *gpsB* Mutations Indicate That GpsB Mediates Protein Phosphorylation and Penicillin-Binding Protein Interactions in *Streptococcus pneumoniae* D39. *Mol Microbiol*. 2017; 103: 931–957. <https://doi.org/10.1111/mmi.13613> PMID: 28010038
35. Cleverley RM, Rutter ZJ, Rismondo J, Corona F, Tsui H-CT, Alatawi FA, et al. The cell cycle regulator GpsB functions as cytosolic adaptor for multiple cell wall enzymes. *Nat Commun*. 2019; 10: 261. <https://doi.org/10.1038/s41467-018-08056-2> PMID: 30651563
36. Claessen D, Emmins R, Hamoen LW, Daniel RA, Errington J, Edwards DH. Control of the cell elongation-division cycle by shuttling of PBP1 protein in *Bacillus subtilis*. *Mol Microbiol*. 2008; 68: 1029–1046. <https://doi.org/10.1111/j.1365-2958.2008.06210.x> PMID: 18363795
37. Mistou M-Y, Sutcliffe IC, van Sorge NM. Bacterial glycobiology: rhamnose-containing cell wall polysaccharides in Gram-positive bacteria. *FEMS Microbiol Rev*. 2016; 40: 464–79. <https://doi.org/10.1093/femsre/fuw006> PMID: 26975195
38. Beek SL van der, Breton YL, Ferenbach AT, Chapman RN, Aalten DMF, Navratilova I, et al. GacA is essential for Group A *Streptococcus* and defines a new class of monomeric dTDP-4-dehydrorhamnose reductases (RmID). *Mol Microbiol*. 2015; 98: 946–962. <https://doi.org/10.1111/mmi.13169> PMID: 26278404
39. Ma Y, Pan F, McNeil M. Formation of dTDP-Rhamnose Is Essential for Growth of Mycobacteria. *J Bacteriol*. 2002; 184: 3392–3395. <https://doi.org/10.1128/JB.184.12.3392-3395.2002> PMID: 12029057
40. Beek SL van der, Zorzoli A, Çanak E, Chapman RN, Lucas K, Meyer BH, et al. Streptococcal dTDP-L-rhamnose biosynthesis enzymes: functional characterization and lead compound identification. *Mol Microbiol*. 2019; 111: 951–964. <https://doi.org/10.1111/mmi.14197> PMID: 30600561
41. Quivey RG, Grayhack EJ, Faustoferri RC, Hubbard CJ, Baldeck JD, Wolf AS, et al. Functional profiling in *Streptococcus mutans*: construction and examination of a genomic collection of gene deletion mutants. *Mol Oral Microbiol*. 2015; 30: 474–495. <https://doi.org/10.1111/omi.12107> PMID: 25973955

42. Kovacs CJ, Faustoferri RC, Quivey RG. RgpF Is Required for Maintenance of Stress Tolerance and Virulence in *Streptococcus mutans*. *J Bacteriol.* 2017;199. <https://doi.org/10.1128/JB.00497-17> PMID: 28924033
43. De A, Liao S, Bitoun JP, Roth R, Beatty WL, Wu H, et al. Deficiency of RgpG Causes Major Defects in Cell Division and Biofilm Formation, and Deficiency of LytR-CpsA-Psr Family Proteins Leads to Accumulation of Cell Wall Antigens in Culture Medium by *Streptococcus mutans*. *Appl Environ Microbiol.* 2017;83. <https://doi.org/10.1128/AEM.00928-17> PMID: 28687645
44. Boyle EA, Andreasson JOL, Chircus LM, Sternberg SH, Wu MJ, Guegler CK, et al. High-throughput biochemical profiling reveals sequence determinants of dCas9 off-target binding and unbinding. *Proc Natl Acad Sci.* 2017; 114: 5461–5466. <https://doi.org/10.1073/pnas.1700557114> PMID: 28495970
45. Anderson EM, Haupt A, Schiel JA, Chou E, Machado HB, Strezoska Ž, et al. Systematic analysis of CRISPR–Cas9 mismatch tolerance reveals low levels of off-target activity. *J Biotechnol.* 2015; 211: 56–65. <https://doi.org/10.1016/j.jbiotec.2015.06.427> PMID: 26189696
46. Klein M, Eslami-Mossallam B, Arroyo DG, Depken M. Hybridization Kinetics Explains CRISPR-Cas Off-Targeting Rules. *Cell Rep.* 2018; 22: 1413–1423. <https://doi.org/10.1016/j.celrep.2018.01.045> PMID: 29425498
47. Chatterjee P, Jakimo N, Jacobson JM. Minimal PAM specificity of a highly similar SpCas9 ortholog. *Sci Adv.* 2018; 4: eaau0766. <https://doi.org/10.1126/sciadv.aau0766> PMID: 30397647
48. Jakimo N, Chatterjee P, Nip L, Jacobson JM. A Cas9 with Complete PAM Recognition for Adenine Dinucleotides. *bioRxiv.* 2018; 429654. <https://doi.org/10.1101/429654>
49. Edraki A, Mir A, Ibraheim R, Gainetdinov I, Yoon Y, Song C-Q, et al. A Compact, High-Accuracy Cas9 with a Dinucleotide PAM for In Vivo Genome Editing. *Mol Cell.* 2019; 73: 714–726.e4. <https://doi.org/10.1016/j.molcel.2018.12.003> PMID: 30581144
50. Bailey J, Cass J, Gasper J, Ngo N-D, Wiggins P, Manoel C. Essential gene deletions producing gigantic bacteria. *PLOS Genet.* 2019; 15: e1008195. <https://doi.org/10.1371/journal.pgen.1008195> PMID: 31181062
51. Kawai Y, Mercier R, Mickiewicz K, Serafini A, Carvalho LPS de, Errington J. Crucial role for central carbon metabolism in the bacterial L-form switch and killing by β -lactam antibiotics. *Nat Microbiol.* 2019; 1–11. <https://doi.org/10.1038/s41564-018-0331-3>
52. Nakano K, Nomura R, Nakagawa I, Hamada S, Ooshima T. Demonstration of *Streptococcus mutans* with a Cell Wall Polysaccharide Specific to a New Serotype, k, in the Human Oral Cavity. *J Clin Microbiol.* 2004; 42: 198–202. <https://doi.org/10.1128/JCM.42.1.198-202.2004> PMID: 14715753
53. Coykendall AL. Classification and identification of the viridans streptococci. *Clin Microbiol Rev.* 1989; 2: 315–328. <https://doi.org/10.1128/cmr.2.3.315> PMID: 2670193
54. Beaussart A, Péchoux C, Trieu-Cuot P, Hols P, Mistou M-Y, F., Dufrière Y. Molecular mapping of the cell wall polysaccharides of the human pathogen *Streptococcus agalactiae*. *Nanoscale.* 2014; 6: 14820–14827. <https://doi.org/10.1039/c4nr05280c> PMID: 25358409
55. Caliot É, Dramsi S, Chapot-Chartier M-P, Courtin P, Kulakauskas S, Péchoux C, et al. Role of the Group B antigen of *Streptococcus agalactiae*: a peptidoglycan-anchored polysaccharide involved in cell wall biogenesis. *PLoS Pathog.* 2012; 8: e1002756. <https://doi.org/10.1371/journal.ppat.1002756> PMID: 22719253
56. Terleckyj B, Willett NP, Shockman GD. Growth of several cariogenic strains of oral streptococci in a chemically defined medium. *Infect Immun.* 1975; 11: 649–655. PMID: 1091546
57. Zhang Q, Ye Y. Not all predicted CRISPR–Cas systems are equal: isolated *cas* genes and classes of CRISPR like elements. *BMC Bioinformatics.* 2017; 18: 92. <https://doi.org/10.1186/s12859-017-1512-4> PMID: 28166719
58. Biswas A, Gagnon JN, Brouns SJJ, Fineran PC, Brown CM. CRISPRTarget. *RNA Biol.* 2013; 10: 817–827. <https://doi.org/10.4161/rna.24046> PMID: 23492433
59. Crooks GE, Hon G, Chandonia J-M, Brenner SE. WebLogo: a sequence logo generator. *Genome Res.* 2004; 14: 1188–90. <https://doi.org/10.1101/gr.849004> PMID: 15173120
60. Blin K, Pedersen LE, Weber T, Lee SY. CRISPy-web: An online resource to design sgRNAs for CRISPR applications. *Synth Syst Biotechnol.* 2016; 1: 118–121. <https://doi.org/10.1016/j.synbio.2016.01.003> PMID: 29062934
61. Lorenz R, Bernhart SH, Höner zu Siederdissen C, Tafer H, Flamm C, Stadler PF, et al. ViennaRNA Package 2.0. *Algorithms Mol Biol.* 2011; 6: 26. <https://doi.org/10.1186/1748-7188-6-26> PMID: 22115189
62. Jong IG de, Beilharz K, Kuipers OP, Veening J-W. Live Cell Imaging of *Bacillus subtilis* and *Streptococcus pneumoniae* using Automated Time-lapse Microscopy. *JoVE J Vis Exp.* 2011; e3145. <https://doi.org/10.3791/3145> PMID: 21841760

63. Abranches J, Miller JH, Martinez AR, Simpson-Haidaris PJ, Burne RA, Lemos JA. The collagen-binding protein Cnm is required for *Streptococcus mutans* adherence to and intracellular invasion of human coronary artery endothelial cells. *Infect Immun*. 2011; 79: 2277–2284. <https://doi.org/10.1128/IAI.00767-10> PMID: [21422186](https://pubmed.ncbi.nlm.nih.gov/21422186/)